JACS
JOURNAL OF THE AMERICAN CHEMICAL SOCIETY
Communication
Cite This: J. Am. Chem. Soc. 2019, 141, 4505−4509
pubs.acs.org/JACS

Thermal Emitting Strategy to Synthesize Atomically Dispersed Pt Metal Sites from Bulk Pt Metal

Yunteng Qu,[†] Bingxu Chen,[§] Zhijun Li,[†] Xuezhi Duan,*[,§] Liguang Wang,[∥] Yue Lin,[⊥] Tongwei Yuan,[#] Fangyao Zhou,[†] Yidong Hu,[†] Zhengkun Yang,[†] Changming Zhao,[†] Jing Wang,[†] Chao Zhao,[†] Yanmin Hu,[†] Geng Wu,[†] Qinghua Zhang,[¶] Qian Xu,[⊗] Bingyao Liu,[▽] Peng Gao,[▽,◆] Rui You,[†,⊥] Weixin Huang,[†,⊥] Lirong Zheng,[☆] Lin Gu,[¶] Yuen Wu,*[,†] and Yadong Li[‡]

[†]School of Chemistry and Materials Science, Hefei National Laboratory for Physical Sciences at the Microscale, University of Science and Technology of China, Hefei 230026, China
[‡]Department of Chemistry, Tsinghua University, Beijing 100084, China
[§]State Key Laboratory of Chemical Engineering, East China University of Science and Technology, Shanghai 200237, China
[∥]Department of Physics, City University of Hong Kong, Hong Kong, China
[⊥]CAS Key Laboratory of Materials for Energy Conversion and Department of Chemical Physics, University of Science and Technology of China, Hefei 230026, China
[#]NEST Lab, Department of Chemistry, College of Science, Shanghai University, Shanghai 200444, China
[¶]Institute of Physics, Chinese Academy of Sciences, Beijing 100190, China
[⊗]National Synchrotron Radiation Laboratory, University of Science and Technology of China, Hefei 230026, China
[☆]Institute of High Energy Physics, Beijing 100049, China
[▽]Electron Microscopy Laboratory and International Center for Quantum Materials, School of Physics, Academy for Advanced Interdisciplinary Studies, Peking University, Beijing 100871, China
[◆]Collaborative Innovation Centre of Quantum Matter, Beijing 100871, China

Supporting Information

ABSTRACT: Developing a facile route to access active and well-defined single atom sites catalysts has been a major area of focus for single atoms catalysts (SACs). Herein, we demonstrate a simple approach to generate atomically dispersed platinum via a thermal emitting method using bulk Pt metal as a precursor, significantly simplifying synthesis routes and minimizing synthesis costs. The ammonia produced by pyrolysis of Dicyandiamide can coordinate with platinum atoms by strong coordination effect. Then, the volatile $Pt(NH_3)_x$ can be anchored onto the surface of defective graphene. The as-prepared Pt SAs/DG exhibits high activity for the electrochemical hydrogen evolution reaction and selective oxidation of various organosilanes. This viable thermal emitting strategy can also be applied to other single metal atoms, for example, gold and palladium. Our findings provide an enabling and versatile platform for facile accessing SACs toward many industrial important reactions.

Single-atom catalysts (SACs) have become an area of growing scientific interest owing to their maximum atom efficiency and highly catalytic performance.[1−9] Recently, some synthetic strategies have been reported to fabricate SACs. In particular, wet-chemical approaches, including coprecipitation and impregnation methods etc., are widely employed because of their low cost and ease of operation.[10−12] However, these approaches suffer from the drawbacks of fusion/aggregation of metal species during the synthetic processes, which greatly hinders their practical applications. Furthermore, other synthetic strategies, such as atomic layer deposition (ALD)[13] and mass-selected soft landing,[14] commonly require expensive equipment with low yields, which are not feasible for large-scale production. Therefore, development of a facile and practical strategy for the synthesis of SACs with high activity and well-defined sites is particularly attractive in the field.

Recently, only a few top-down strategies have been reported for preparing SACs using metal nanoparticles as the precursor.[15] These works involve the transformation from nanoparticles to single atoms under thermal treatment, simplifying the synthesis routes for SACs.[16,17] Currently, our group demonstrated that the Ni atoms of Ni foil could diffuse into the melamine film, forming hierarchical carbon papers with the existence of Ni SAs and Ni NPs.[18] Nevertheless, direct fabrication of SACs from bulk noble metal materials have been rarely reported.

Herein, we demonstrate a facile thermal emitting strategy to synthesize Pt single sites catalyst directly from bulk Pt net. The preparation procedure and proposed formation mechanism are shown in Figure 1a and Figure S1. Dicyandiamide (DCD), Pt net and graphene oxidation (GO) were sequentially placed in a porcelain boat with Ar flow and then the porcelain boat was

Received: September 12, 2018
Published: March 5, 2019

DOI: 10.1021/jacs.8b09834
J. Am. Chem. Soc. 2019, 141, 4505−4509

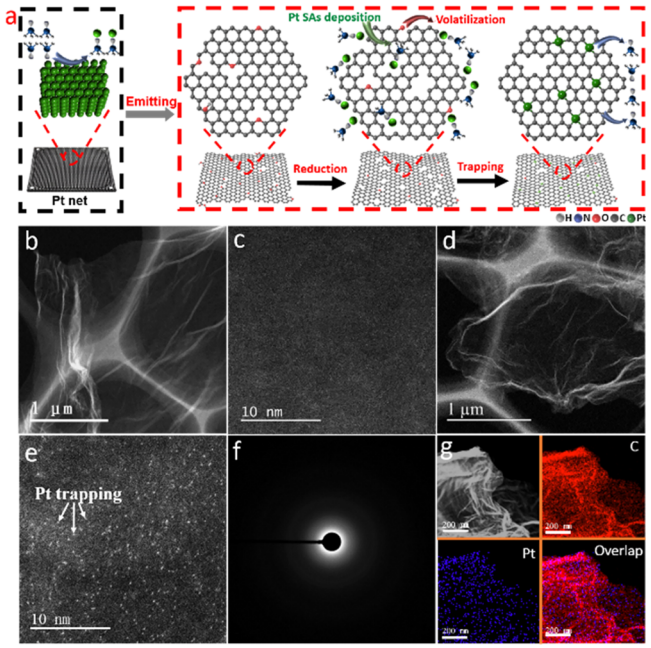

Figure 1. (a) Proposed reaction mechanism for the preparation of Pt SAs/DG. (b) HAADF STEM image and (c) magnified HAADF STEM image of DG. (d) HAADF STEM image and (e) magnified HAADF STEM image of Pt SAs/DG. (f) Corresponding EELS element mapping of Pt SAs/DG and (g) SAED pattern of Pt SAs/DG.

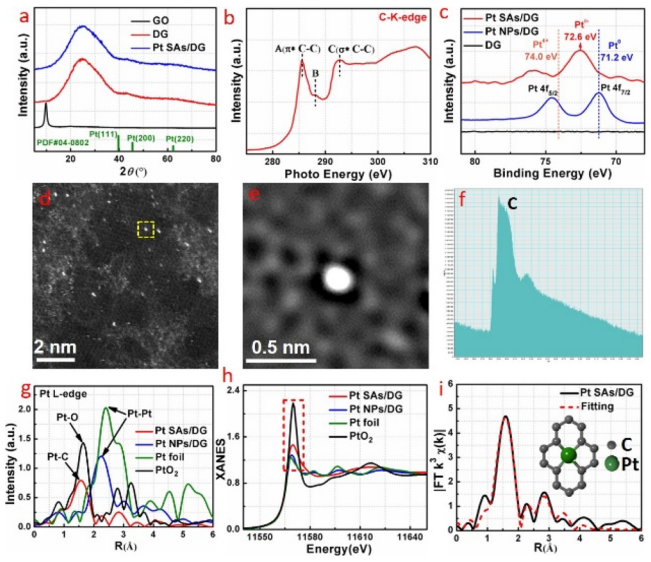

Figure 2. (a) XRD patterns of Pt SAs/DG, DG, and graphene oxidation. (b) C−K-edge NEXAFS spectrum of Pt SAs/DG. (c) Pt 4f XPS spectra of the Pt SAs/DG, DG, and Pt NPs/DG. (d) High-resolution HADDF-STEM image of Pt SAs/DG. (e) Zoomed-in image of the defective area marked with the yellow dashed frame in panel d. (f) Corresponding EELS point spectrum from yellow dashed frame atom in panel d. (g) R-space spectra from EXAFS. (h) Pt L-edge XANES spectra. (i) Corresponding EXAFS fitting curve for Pt SAs/DG. Inset is the proposed Pt−C coordination environment.

heated to 1100 °C. Under high temperature, the DCD underwent a pyrolysis process to generate ammonia gas.[19,20] Based on strong coordination interaction between ammonia and Pt atoms, the possible volatile $Pt(NH_3)_x$ species were formed. Meanwhile, the Pt^0 species may be oxidized by

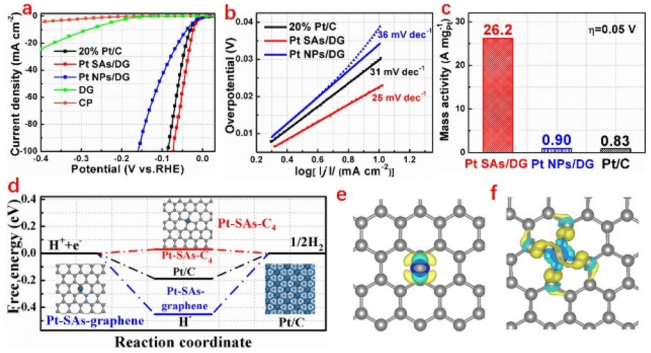

Figure 3. (a) HER linear sweep voltammetry (LSV) curves of the catalysts. (b) Corresponding Tafel plots and mass activity of Pt SAs/DG, Pt NPs/DG, and commercial Pt/C. (d) Calculated Gibbs free energy diagram of HER on Pt/C, Pt-SAs-graphene and Pt-SAs-C_4 at the equilibrium potential. The charge density difference of Pt SAs supported on the (e) pristine graphene and (f) double-vacant graphene (Pt-SAs-C_4). Light blue and yellow isosurfaces denote a decrease and increase of 0.01 e/Å^3 for electronic density, respectively.

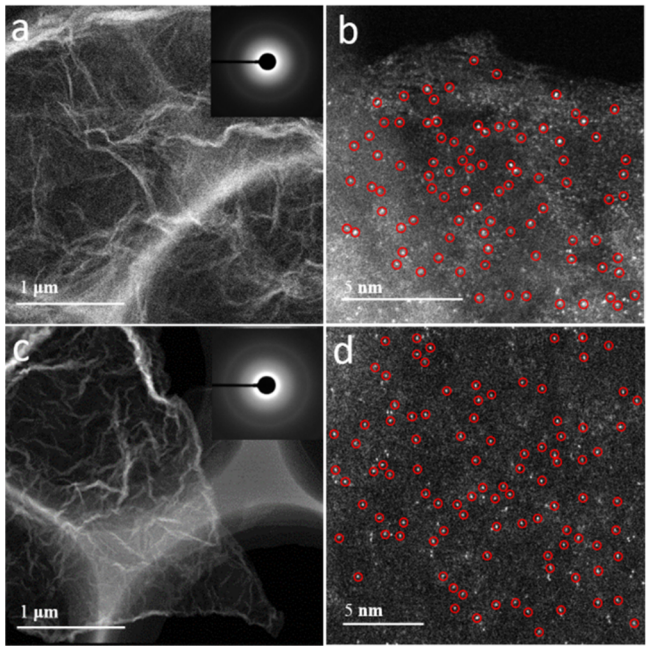

Figure 4. (a) HAADF STEM, (b) magnified HAADF STEM images of Pd SAs/DG; (c) HAADF STEM, (d) magnified HAADF STEM images of Au SAs/DG. Inset is the corresponding SAED pattern of Pd SAs/DG and Au SAs/DG.

oxygen-containing functional group on the surface of GO, forming $Pt^{\delta+}$ ($0 < \delta < 4$) species. Subsequently, the most oxygen-containing functional group on GO were removed through the thermal treatment, generating defective graphene (DG). Then, the $Pt^{\delta+}$ ($0 < \delta < 4$) species were further trapped by the DG, forming the isolated Pt SAs/DG catalysts.

As a control, the GO was reduced to DG in argon at 1100 °C without DCD. Scanning transmission electron microscopy (STEM) (Figure 1b) and aberration-corrected HAADF STEM (Figure 1c) reveal metal atoms cannot be observed on DG, suggesting the argon is unable to haul the Pt atoms out of bulk Pt. When DCD is introduced, isolated Pt atoms (bright spots) on DG can be clearly identified according to aberration-corrected HAADF STEM images (Figure 1d,e, Figures S2 and

DOI: 10.1021/jacs.8b09834
J. Am. Chem. Soc. 2019, 141, 4505−4509

S3). Additionally, low-magnified TEM image indicates that there is no observable Pt NPs in Pt SAs/DG (Figure S4), in line with the ring-like selected-area electron diffraction (SAED) pattern (Figure 1f). Figure 1g shows the HADDF STEM image and corresponding Pt, and C elemental mappings of Pt SAs/DG by EELS, revealing the Pt was homogeneously dispersed over the DG. The above results strongly support the successful emitting of Pt atoms from the bulk metal and the trapping by the DG. Note that a higher temperature (1200 °C) lead to the formation of Pt NPs (Figures S5 and S6). Correspondingly, the color of the samples was evolved from yellow to black (Figure S7).

Obviously, GO exhibits a characteristic peak at 9° (Figure 2a). For Pt SAs/DG, the disappearance of the peak at 9° indicates the reduction of GO. Moreover, no observable Pt characteristic peaks are found, demonstrating the absence of crystalline Pt. Due to the lack of N source, one cannot observe the discernible peak of N 1s for DG (Figure S8a). Interestingly, both Pt SAs/DG and Pt NPs/DG, as shown in Figures S9 and S10, exhibit ultralow contents of N (∼1.0 at. %). This can be attributed to the instable bonding configurations of N−C under high temperature. Therefore, we assume that most of the Pt single atoms were anchored on the defective carbon sites. Noteworthy, the Pt SAs/DG show a higher I_D/I_G value compared with the control sample in Raman measurement (Figure S11). G band is assigned to the E_{2g} phonon of C sp^2 atoms, while D band is a breathing mode of k-point phonons of A_{1g} symmetry.[21] The increased I_D/I_G shows a decrease in the average size of the sp^2 domains, indicating more carbon defect sites. Thus, this implies the volatilization of N atoms would create abundant defect sites of carbon. Near edge X-ray absorption fine structure (NEXAFS) shows the C K-edge spectrum of Pt SAs/DG exhibits the negligible peak B was attributed to C−O−C or C−N−C,[22,23] further indicating the limited N sites in Pt SAs/DG. Furthermore, as shown in Figure 2c, the binding energy of the Pt $4f_{7/2}$ and $4f_{5/2}$ peak for Pt SAs/DG is at 72.6 and 75.7 eV corresponding to the $Pt^{\delta+}$ ($0 < \delta < 4$).[24]

High-resolution HADDF-STEM (Figure 2d) measurement was employed to further confirm the anchored sites of Pt atoms.[25] The Divacancy with trapped Pt atom was clearly observed in Figure 2e. The corresponding EELS point spectrum show the N element was absent around Pt atom (Figure 2f), further confirming that Pt single atoms were anchored on the defective carbon sites. X-ray absorption of fine structure (XAFS) show the Pt L_3-edge of the as-prepared samples (Pt SAs/DG, Pt NPs/DG) and reference (Pt foil and PtO_2). The R-space spectrum of the EXAFS, as shown in Figure 2g, exhibits a main peak around 1.98 Å, which matches the bond length of Pt−C. As a control, Pt foil show a prominent peak at 2.78 Å which belongs to the Pt−Pt coordination. Notably, Pt NPs/DG show a shorter bond length of Pt−Pt (2.62 Å) compared with Pt foil, in line with the theoretical predicted results.[1,26] X-ray absorption near-edge structure (XANES) spectra (Figure 2h) show the white-line intensity of Pt SAs/DG located between Pt foil and PtO_2, demonstrating the oxidation state of Pt ($Pt^{\delta+}$, $0 < \delta < 4$)) in Pt SAs/DG. The fitting results of R-space spectrum for Pt SAs/DG depicts the proposed coordination structure of $Pt-C_4$ (Figure 2i and Table S1).

The HER performance of the Pt SAs/DG, Pt NPs/DG, and commercial Pt/C was investigated in N_2-saturated 0.5 M H_2SO_4. Electrochemical impedance spectroscopy (EIS) was employed to correct the solution resistance (Figure S12). The contents in Pt SAs/DG and Pt NPs/DG are measured to be 2.1 and 8.6 wt % (Table S2), as identified by inductively coupled plasma atomic emission spectroscopy (ICP-AES). The bare CP and DG display a poor HER activity (Figure 3a). Impressively, the Pt SAs/DG achieved the highest electrocatalytic activity when the reaction time was 5 h (Figure S13). The overpotential (at 10 mA cm^{-2}) for Pt SAs/DG is 23 mV, which is lower than Pt/C (30 mV) and Pt NPs/DG (38 mV). Figure 3b reveals the Tafel slope of the Pt SAs/DG is 25 mV $decade^{-1}$, indicating that even faster electron-transfer process than commercial Pt/C (30 mV $decade^{-1}$). Moreover, the HER activity at a −0.05 V for the Pt SAs/DG is 26.2 A mg^{-1}_{Pt}, 31.5 times greater than that of the commercial Pt/C (0.83 A mg^{-1}_{Pt}) (Figure 3c). Furthermore, Pt SAs/DG also outperformed the Pt SACs prepared by ALD or impregnation method and most previously reported HER catalysts (Table S3). Specially, Pt SAs/DG has also show higher HER activity compared with Pt/C in alkaline media (Figure S14).

Additionally, an essentially identical catalytic performance can be observed for Pt SAs/DG despite the different amounts of precursors were used (Figure S15). After 5000 CV cycles, the Pt SAs/DG shows an insignificant attenuation compared with the obvious degradation for commercial Pt/C (Figure S16a,b). Next, the current density displays a negligible decrease at a −0.023 V after 24 h (Figure S16c). Examination of HAADF STEM images and EXAFS result confirmed the atomically isolated Pt atoms retained after the durability tests (Figure S17). Together, these results imply a strong electrocatalytic stability of the Pt SAs/DG catalyst due to the robust $Pt-C_4$ coordination structure.

Considering the Pt−C coordination environment of the Pt SAs, the model of Pt-SAs-C_4 is constructed (Figure S18). The Pt−C bond distance of the Pt-SAs-C_4 is 1.98 Å, in accordance with the EXAFS observation (Table S1). The models of the Pt (111) surface and Pt SAs supported on the pristine graphene are also constructed. The Pt SAs prefers to anchor on the DG compared to the pristine graphene based on the much negative binding energy over the Pt-SAs-C_4 (Table S4). The Gibbs free energies for H adsorption (ΔG_H*) are calculated over the three models as shown in Figure 3d.[27,28] Interestingly, the calculated ΔG_H* value of the Pt-SAs-C_4 was close to zero, i.e., 0.03 eV, strongly indicating the enhanced HER activity over Pt SAs/DG. Furthermore, charge analysis show that much larger charge transfer appears between the Pt SAs and the DG compared to the pristine graphene (Figure 3e and f, Table S4). This leads to more mediate ΔG_H* to promote the overall HER performance for Pt SAs/DG. PtN_x ($x = 1-4$) models have also been established in Figure S19. The PtN_x show either too negative or positive ΔG_H* (Table S5) compared with Pt(111) and thus poor HER activity.

In addition, the as-prepared Pt SAs/DG was demonstrated to be a highly active and selective catalyst in the oxidation of various organosilanes (Figure S20). Dimethylphenylsilane was transformed to dimethylphenylsilanol within 75 min without byproduct except H_2. In the reaction, the turn over frequency (TOF) was 4367 h^{-1} for the Pt SAs/DG. Moreover, the Pt SAs/DG catalyst retained high activity and selectivity after five cycles. The Pt SAs/DG also show excellent selectivity and conversion efficiency in the oxidation of other types of silanes.

Other bulk metal precursors (Au and Pd) were also employed to test the generality of this thermal emitting method. HAADF STEM images clearly show individual bright

DOI: 10.1021/jacs.8b09834
J. Am. Chem. Soc. 2019, 141, 4505−4509

dots in Pd SAs/DG (Figure 4a,b and Figures S21−S23) and Au SAs/DG (Figure 4c,d and Figures S24−S26). The XRD pattern (Figure S27) and SAED (Figure 4a,c inset) further demonstrate the atomically dispersed gold and palladium atoms can be successfully stabilized on DG.

In summary, an efficient and simple thermal emitting strategy that transforms bulk noble metals into metal SA catalysts was developed and validated. Importantly, the introduction of ammonia molecules engenders an advantages approach to effectively haul out Pt atoms from bulk form and anchor them onto the DG. The resultant Pt SAs/DG catalyst has shown superior performance for HER and the oxidation of various organosilanes. These new findings provide valuable guidance for the direct/facile preparation of SACs from bulk metals, showing great potential to scale up the production of SACs toward various industrial applications.

■ ASSOCIATED CONTENT

Supporting Information

The Supporting Information is available free of charge on the ACS Publications website at DOI: 10.1021/jacs.8b09834.

Detailed experimental procedures; SEM and TEM images; XRD data; XPS data (PDF)

■ AUTHOR INFORMATION

Corresponding Authors

*xzduan@ecust.edu.cn
*yuenwu@ustc.edu.cn

ORCID

Xuezhi Duan: 0000-0002-5843-5950
Yue Lin: 0000-0001-5333-511X
Peng Gao: 0000-0003-0860-5525
Weixin Huang: 0000-0002-5025-3124
Lin Gu: 0000-0002-7504-031X
Yuen Wu: 0000-0001-9524-2843

Author Contributions

Y.Q., B.C. and Z.L. contributed equally.

Notes

The authors declare no competing financial interest.

■ ACKNOWLEDGMENTS

This work was supported by National Key R&D Program of China 2017YFA (0208300) and (0700104), the National Natural Science Foundation of China (21522107, 21671180), the State Key Laboratory of Organic Inorganic Composites (oic-201801007). We thank the photoemission endstations BL1W1B in Beijing Synchrotron Radiation Facility (BSRF), BL14W1 in Shanghai Synchrotron Radiation Facility (SSRF), and BL10B and BL11U in National Synchrotron Radiation Laboratory (NSRL) for the help in characterizations.

■ REFERENCES

(1) Liu, J.; Jiao, M.; Lu, L.; Barkholtz, H. M.; Li, Y.; Wang, Y.; Jiang, L.; Wu, Z.; Liu, D.-j.; Zhuang, L. High Performance Platinum Single Atom Electrocatalyst for Oxygen Reduction Reaction. *Nat. Commun.* **2017**, *8*, 1−9.

(2) Nie, L.; Mei, D.; Xiong, H.; Peng, B.; Ren, Z.; Hernandez, X. I. P.; DeLaRiva, A.; Wang, M.; Engelhard, M. H.; Kovarik, L.; et al. Activation of Surface Lattice Oxygen in Single-Atom Pt/CeO_2 for Low-temperature CO Oxidation. *Science* **2017**, *358*, 1419−1423.

(3) Qiao, B.; Wang, A.; Yang, X.; Allard, L. F.; Jiang, Z.; Cui, Y.; Liu, J.; Li, J.; Zhang, T. Single-atom Catalysis of CO Oxidation Using Pt_1/FeO_x. *Nat. Chem.* **2011**, *3*, 634−641.

(4) Yin, P.; Yao, T.; Wu, Y.; Zheng, L.; Lin, Y.; Liu, W.; Ju, H.; Zhu, J.; Hong, X.; Deng, Z.; et al. Single Cobalt Atoms with Precise N-Coordination as Superior Oxygen Reduction Reaction Catalysts. *Angew. Chem., Int. Ed.* **2016**, *55*, 10800−10805.

(5) Cheng, N.; Stambula, S.; Wang, D.; Banis, M. N.; Liu, J.; Riese, A.; Xiao, B.; Li, R.; Sham, T.-K.; Liu, L.-M.; et al. Platinum Single-atom and Cluster Catalysis of the Hydrogen Evolution Reaction. *Nat. Commun.* **2016**, *7*, 1−9.

(6) Lin, J.; Wang, X. Rh Single Atom Catalyst for Direct Conversion of Methane to Oxygenates. *Sci. China. Mater.* **2018**, *61*, 758−760.

(7) Yin, X.-P.; Wang, H.-J.; Tang, S.-F.; Lu, X.-L.; Shu, M.; Si, R.; Lu, T.-B. Engineering the Coordination Environment of Single-Atom Pt Anchored on Graphdiyne for Optimizing Electrocatalytic Hydrogen Evolution. *Angew. Chem., Int. Ed.* **2018**, *57*, 9382−9386.

(8) Wang, X.; Chen, Z.; Zhao, X.; Yao, T.; Chen, W.; You, R.; Zhao, C.; Wu, G.; Wang, J.; Huang, W.; Yang, J.; Hong, X.; Wei, S.; Wu, Y.; Li, Y. Regulation of Coordination Number over Single Co Sites: Triggering the Efficient Electroreduction of CO_2. *Angew. Chem.* **2018**, *130*, 1962−1966.

(9) Wang, X.; Wang, W.; Qiao, M.; Wu, G.; Chen, W.; Yuan, T.; Xu, Q.; Chen, M.; Zhang, Y.; Wang, X.; Wang, J.; Ge, J.; Hong, X.; Li, Y.; Wu, Y.; Li, Y. Atomically Dispersed Au_1 Catalyst Towards Efficient Electrochemical Synthesis of Ammonia. *Sci. Bull.* **2018**, *63*, 1246−1253.

(10) Lin, J.; Wang, A.; Qiao, B.; Liu, X.; Yang, X.; Wang, X.; Liang, J.; Li, J.; Liu, J.; Zhang, T. Remarkable Performance of Ir_1/FeO_x Single-atom Catalyst in Water Gas Shift Reaction. *J. Am. Chem. Soc.* **2013**, *135*, 15314−15317.

(11) Lin, L.; Zhou, W.; Gao, R.; Yao, S.; Zhang, X.; Xu, W.; Zheng, S.; Jiang, Z.; Yu, Q.; Li, Y.-W.; et al. Low-temperature Hydrogen Production from Water and Methanol Using Pt/α-MoC Catalysts. *Nature* **2017**, *544*, 80−83.

(12) Liu, P.; Zhao, Y.; Qin, R.; Mo, S.; Chen, G.; Gu, L.; Chevrier, D. M.; Zhang, P.; Guo, Q.; Zang, D.; et al. Photochemical Route for Synthesizing Atomically Dispersed Palladium Catalysts. *Science* **2016**, *352*, 797−800.

(13) Peters, A. W.; Li, Z.; Farha, O. K.; Hupp, J. T. Atomically Precise Growth of Catalytically Active Cobalt Sulfide on Flat Surfaces and Within a Metal−Organic Framework via Atomic Layer Deposition. *ACS Nano* **2015**, *9*, 8484−8490.

(14) Abbet, S.; Sanchez, A.; Heiz, U.; Schneider, W.-D.; Ferrari, A. M.; Pacchioni, G.; Rösch, N. Acetylene Cyclotrimerization on Supported Size-selected Pd n Clusters (1≤ n≤ 30): One Atom is Enough! *J. Am. Chem. Soc.* **2000**, *122*, 3453−3457.

(15) Li, Z.; Wang, D.; Wu, Y.; Li, Y. Recent Advances in the Precise Control of Isolated Single Site Catalysts by Chemical Methods. *Natl. Sci. Rev.* **2018**, *5*, 673−689.

(16) Jones, J.; Xiong, H.; DeLaRiva, A. T.; Peterson, E. J.; Pham, H.; Challa, S. R.; Qi, G.; Oh, S.; Wiebenga, M. H.; Hernández, X. I. P.; et al. Thermally Stable Single-atom Platinum-on-ceria Catalysts via Atom Trapping. *Science* **2016**, *353*, 150−154.

(17) Wei, S.; Li, A.; Liu, J.-C.; Li, Z.; Chen, W.; Gong, Y.; Zhang, Q.; Cheong, W.-C.; Wang, Y.; Zheng, L.; et al. Direct Observation of Noble Metal Nanoparticles Transforming to Thermally Stable Single Atoms. *Nat. Nanotechnol.* **2018**, *13*, 856−861.

(18) Zhao, C.; Wang, Y.; Li, Z.; Chen, W.; Xu, Q.; He, D.; Xi, D.; Zhang, Q.; Yuan, T.; Qu, Y. Solid-Diffusion Synthesis of Single-Atom Catalysts Directly from Bulk Metal for Efficient CO_2 Reduction. *Joule* **2018**, *3*, 584−594.

(19) Ong, W.-J.; Tan, L.-L.; Ng, Y. H.; Yong, S.-T.; Chai, S.-P. Graphitic carbon nitride (g-C_3N_4)-based Photocatalysts for Artificial Photosynthesis and Environmental Remediation: Are We a Step Closer to Achieving Sustainability? *Chem. Rev.* **2016**, *116*, 7159−7329.

(20) Martin, D. J.; Qiu, K.; Shevlin, S. A.; Handoko, A. D.; Chen, X.; Guo, Z.; Tang, J. Highly Efficient Photocatalytic H_2 Evolution from

DOI: 10.1021/jacs.8b09834
J. Am. Chem. Soc. 2019, 141, 4505−4509

Water Using Visible Light and Structure-Controlled Graphitic Carbon Nitride. *Angew. Chem., Int. Ed.* **2014**, *53*, 9240−9245.
(21) Suenaga, K.; Yudasaka, M.; Colliex, C.; Iijima, S. Radially Modulated Nitrogen Distribution in CN_x Nanotubular Structures Prepared by CVD Using Ni Phthalocyanine. *Chem. Phys. Lett.* **2000**, *316*, 365−372.
(22) Zhang, L.-S.; Liang, X.-Q.; Song, W.-G.; Wu, Z.-Y. Identification of the Nitrogen Species on N-doped Graphene Layers and Pt/NG Composite Catalyst for Direct Methanol Fuel Cell. *Phys. Chem. Chem. Phys.* **2010**, *12*, 12055−12059.
(23) Liang, Y.; Li, Y.; Wang, H.; Zhou, J.; Wang, J.; Regier, T.; Dai, H. Co_3O_4 Nanocrystals on Graphene as a Synergistic Catalyst for Oxygen Reduction Reaction. *Nat. Mater.* **2011**, *10*, 780−786.
(24) Guo, L.; Jiang, W.-J.; Zhang, Y.; Hu, J.-S.; Wei, Z.-D.; Wan, L.-J. Embedding Pt Nanocrystals in N-Doped Porous Carbon/carbon nanotubes toward Highly Stable Electrocatalysts for the Oxygen Reduction Reaction. *ACS Catal.* **2015**, *5*, 2903−2909.
(25) Zhang, L.; Jia, Y.; Gao, G.; Yan, X.; Chen, N.; Chen, J.; Soo, M. T.; Wood, B.; Yang, D.; Du, A.; et al. Graphene Defects Trap Atomic Ni Species for Hydrogen and Oxygen Evolution Reactions. *Chem.* **2018**, *4*, 285−297.
(26) Chang, J.; Koningsberger, D.; Gates, B. Structurally Simple Supported Platinum Clusters Prepared from $[Pt_{15}(CO)_{30}]_2$-on Magnesium Oxide. *J. Am. Chem. Soc.* **1992**, *114*, 6460−6466.
(27) Nørskov, J. K.; Bligaard, T.; Rossmeisl, J.; Christensen, C. H. Towards the Computational Design of Solid Catalysts. *Nat. Chem.* **2009**, *1*, 37−46.
(28) Nørskov, J. K.; Bligaard, T.; Logadottir, A.; Kitchin, J.; Chen, J. G.; Pandelov, S.; Stimming, U. Trends in the Exchange Current for Hydrogen Evolution. *J. Electrochem. Soc.* **2005**, *152*, J23−J26.

DOI: 10.1021/jacs.8b09834
J. Am. Chem. Soc. 2019, 141, 4505−4509